Catalysis Today 181 (2012) 68–74

Contents lists available at ScienceDirect

Catalysis Today

journal homepage: www.elsevier.com/locate/cattod

Reversible oxidation of WO_x and MoO_x nano phases

S. Bruyère[a,1], B. Domenichini[a], K. Schierbaum[b], Z. Li[c], S. Bourgeois[a,*]

[a] ICB, UMR 5209 CNRS-Université de Bourgogne, 9 Av. A. Savary, BP 47870, F-21078 Dijon Cedex, France
[b] Institut für Experimentelle Physik der kondensierten Materie, Heinrich-Heine Universität Düsseldorf, Universitätsstrasse 1, D-40225 Düsseldorf, Germany
[c] ISA, University of Aarhus, Ny Munkegade, DK-8000, Aarhus C, Denmark

ARTICLE INFO

Article history:
Received 25 February 2011
Received in revised form 4 May 2011
Accepted 27 June 2011
Available online 28 July 2011

Keywords:
WO_x
MoO_x
TiO_2
Photoemission
Oxygen exposure
Gas sensing

ABSTRACT

WO_x and MoO_x nano phases were prepared on TiO_2(1 1 0) surfaces by a CVD procedure consisting of adsorption and decomposition of $W(CO)_6$ or $Mo(CO)_6$ precursors followed by annealing under UHV. Metal amount involved in each elaborated sample is in the fractional range from 0.1 to 0.35 equivalent monolayer (eqML) of W or Mo. Evolution of sample stoichiometry as a function of subsequent treatment is followed by valence band and core level photoemission as well as work function measurement. In each case, exposure of samples to molecular oxygen at room temperature induces an increase of sample work function in a range of several tenth of eV. Such a work function change is related to oxidation of sample involving both titanium and tungsten (or molybdenum) ions. Such an oxidation is reversible through an annealing under UHV at 470 K for molybdenum oxide and 670 K for tungsten oxide. Several cycles of exposure/annealing are possible without changes in work function or stoichiometry.

1. Introduction

Tungsten oxide (WO_3) or molybdenum oxide (MoO_3) is widely used in diverse applications such as gas sensor and catalysis [1–3]. In catalytic applications MoO_3 or WO_3 are normally supported on different oxides depending on the type of reaction to be catalyzed. The catalyst support provides a surface for the metal/metal oxide dispersion, but, in addition, some of them such as TiO_2 have been shown to be active in the heterogeneous catalytic process itself. Actually the addition of MoO_3 or WO_3 in the formulation of different TiO_2 based catalysts is reported to enhance the catalytic activity both for the total oxidation of various pollutants [4] and in the reduction of NO_x [5,6].

In addition, the development of visible light photocatalysis is an important topic in photocatalysis research today: TiO_2 which is used in photocatalytic oxidation reactions for the rapid degradation of organic pollutants in water and air [7,8] has a wide band gap, close to 3 eV, absorbing thus only a small fraction of solar light. Different ways were found to improve the efficiency of TiO_2 photocatalyst and to extend its light absorption spectra to the visible region, for example the introduction into TiO_2 of either anions [9], or cations [10]. Coupling TiO_2 with another semi-conductor such as WO_3 increases also the efficiency of photocatalytic process by increasing the charge separation and extending the energy range of photoexcitation [11].

Considering sensing properties, WO_3-based semiconducting gas sensors have showed good responses, both to NH_3 and NO [12] or to ozone [13]. However the sensor response depends on physical and chemical properties of sensitive films i.e. on morphology and chemical composition of WO_3 structures.

In order to be able to address the relevant parameters for catalytic or gas sensing reactions properly, model systems were built on planar substrates, suitable for surface science investigation. So, different procedures have been optimized in order to get model catalysts or gas sensors composed of metal oxide clusters supported on planar supports. Supported metal oxide clusters are prepared either via metal evaporation in an oxidizing environment (or by post-oxidation) or by direct sublimation of the oxide [14,15]. In this frame we developed several studies on the growth of refractive metals such as molybdenum or tungsten on TiO_2 surface showing that the growth is driven by two opposite processes: oxidization of deposited atoms due to interfacial reactivity and metal–metal interaction between deposited atoms [16–18]. It is thus quite difficult to control not only deposited metal amount but also deposit composition, in particular the amount of oxygen in the deposit. It was shown that it is easier to control the deposit composition, especially in the case of deposits in the sub monolayer range, when using, instead of classical physical vapour deposition (PVD), kind of chemical vapour deposition (CVD) route with metal hexacarbonyl as a precursor. This route [19] consists in a first step of

* Corresponding author. Tel.: +33 3 80 39 61 50; fax: +33 3 80 39 38 19.
E-mail address: sbourg@u-bourgogne.fr (S. Bourgeois).
[1] Present address: Laboratoire de Réactivité et Chimie des Solides LRCS - UMR 6007, 33 rue St Leu 80039 Amiens, France.

0920-5861/$ – see front matter © 2011 Elsevier B.V. All rights reserved.
doi:10.1016/j.cattod.2011.06.022

precursor adsorption at cryogenic temperature followed by an irradiation step (through photon, ion or electron beams) in order to induce the decomposition of the carbonyl molecule into sub carbonyl species which are more strongly bound to the surface. Subsequent cycles of oxygen exposure/annealing allow total precursor decomposition, organization of nanostructures on the surface and control of the chemical state of obtained phases. In addition, the reaction of metal hexacarbonyl ($M(CO)_6$) with oxides was extensively used to synthesize active catalysts and substantial amount of work [20] has been carried out using a number of techniques to explore the species that are formed from $M(CO)_6$ on high-surface-area oxide supports.

The present work deals with studies of the reactivity towards oxygen of tungsten and molybdenum-based nanostructures on TiO_2(1 1 0) processed using such chemical vapour deposition elaboration way.

2. Experimental

The TiO_2(1 1 0) sample (MaTeck) was prepared by several cycles of Ar^+ sputtering (2.5 keV for 20 min) followed by annealing at 650 °C in UHV (for 10 min). After the annealing, due to the presence of defects into the material, the crystal appears dark blue and is conductive enough to not induce any charging effect. The surface stoichiometry is almost restored through transport of defects to the bulk, which induces a re-oxidation of the surface. The surface oxidation is then completed by an oxygen exposure (200 L) at RT leading to a stoichiometric surface. Such a surface exhibits a sharp (1×1) LEED pattern, proving the good crystallinity of the surface.

$Mo(CO)_6$ (98%, Aldrich) and $W(CO)_6$ (99%, STREM Chemicals) precursors were used to prepare tungsten and molybdenum-based nanostructures by CVD. Details of the procedure are given in Ref. [19].

Photoemission experiments were carried out on SX700 beamline at the ASTRID synchrotron source of the Institute for Storage Ring Facilities (Århus, Denmark). Details on data acquisition are given in [19]. For each sample, in order to take into account possible charging effects and band bending and to correct them, all spectra were referenced to Ti^{4+} component of Ti2p3/2 line fixed at 459.0 eV.

Photoemission was also used to measure changes in the work function of the sample: the contact potential difference between the sample and the energy analyzer was measured by biasing the sample negatively and measuring the minimum energy of secondary electrons. Variations of this threshold can be, in a first approximation, directly linked to modifications of sample work function as far as a conducting sample is considered with no space charge or band bending effects.

Conductance measurements were performed using a gas-flow setup equipped with three mass flow controllers (100 ml/min), electro-polished stainless 1/4 in. tubing and a small stainless chamber with the sample holder. The sample heater consists of a foil, connected to a power supply, which is insulated from the sample by a thin sapphire plate. The temperature is monitored by means of a K-type thermocouple. We used purified nitrogen (99.999%) at a constant flow rate of 50 cm^3/min, streamed through a gas clean filter system to remove oxygen and moisture. The conductance was determined with a Van-der-Pauw electrode arrangement of tantalum contacts, applying a constant current source.

3. Results and discussion

3.1. Tungsten oxide phases

Two kinds of WO_x phases were studied. They were prepared according to procedure exposed in Refs. [21,22] using $W(CO)_6$ carbonyl molecules. According to this procedure, $W(CO)_6$ precursor (from one to several hundreds Langmuir, i.e. from 10 to several thousands seconds at 10^{-7} Torr) is dosed on substrate cooled down 150 K. It results from this exposure the physisorption of 1 eqML for each 10 L of $W(CO)_6$. The system is subsequently irradiated by synchrotron radiation 0-order beam for 5 min inducing partial decomposition of molecules and their chemisorption on the substrate. Molecule decomposition is then completed by subsequent annealing. From W4f/Ti3p area ratio, one can estimate the W amount which was deposited on substrate from comparison to PVD deposits previously performed [16]. These tungsten amounts correspond to ca. 0.15 equivalent monolayer (eqML; according to bcc W structure, 1 eqML is equal to 1.0×10^{15} atoms cm^{-2}) for a series of samples called A obtained using a primary precursor exposure of 10 L and 0.25 eqML for another series of samples called B obtained using a primary precursor exposure of 20 L. The final treatment of all these samples consists in an annealing under UHV at 670 K. These two kinds of tungsten oxide phases are then exposed to molecular oxygen at room temperature in successive steps through 5 orders of magnitude from 0.1 to 10^4 L. Between each steps both sample work function and valence band spectrum are recorded. These measurements are reported in Fig. 1a for the work function of two samples and Fig. 1b for the low binding energy region of the valence band of sample A.

Due to exposures to oxygen extending along several orders of magnitude, work function values are plotted *versus* log of O_2 exposure. The first point corresponds to a measurement before any oxygen exposure and is not involved in curve evolution. As concerns the evolution of work function as function of oxygen exposure, the curve has rough sigmoid shape with a work function increase of ca. 0.5 eV for the two samples on the 6 orders of magnitude which were studied.

In Fig. 1b is shown the low binding energy part of the valence band of the sample. Although rutile titanium dioxide exhibits a 3.0 eV band gap, a feature at ca. 1 eV can be observed in the band gap. Such a feature was always observed for fractional tungsten coverage [16,21] and is composed of both Ti3d and W5d states as previously shown by resonant photoemission spectroscopy [21]. The presence of Ti3d species on an initially stoichiometric TiO_2 surface corresponds to the interaction of metal atoms with oxide surface leading to a reduction of Ti^{4+} cations while W5d states depend upon the amount of deposited tungsten [21]. A clear decrease in the intensity of this feature can be observed while increasing the oxygen exposure. As this feature is related to surface reduced species, its decrease corresponds to sample surface oxidation, such a phenomenon inducing also the work function increase. However, even for highest exposure, states remain in the band gap indicating that the exposure is not high enough to complete the surface oxidation.

After exposure to 10^4 L, samples A and B were submitted to successive subsequent annealing. Work functions of the samples were measured once the samples were cooled down to room temperature. After annealing at 670 K, the recorded values for work functions were pretty close to the ones recorded before the cycle oxygen exposure/annealing: 5.38 eV after the cycle and 5.37 eV before, for sample A, and 5.12 eV compared to 5.11 eV for sample B. Such results seem to indicate a reversibility of sample oxidation induced by annealing. This reversibility is well evidenced in Fig. 2a where are plotted work function changes for sample A after four successive cycles, exposures to 1 L of oxygen and subsequent annealing at 670 K. After exposure to 1 L, the work function is always close to 5.60 eV while annealing leads to a value always equal to ca. 5.38 eV and same values are recorded after each treatment. The same reversible behaviour can be observed on the low binding energy part of the valence band after the same treatments (Fig. 2b). Actually all the spectra after annealing are really close

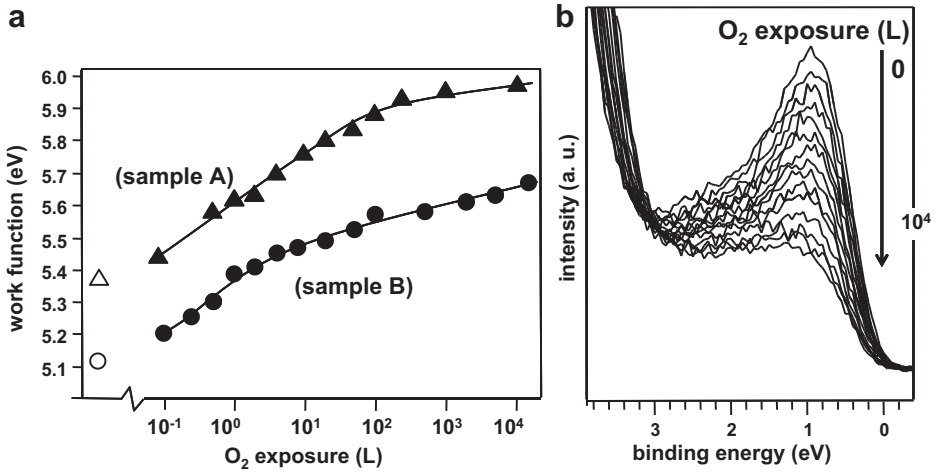

Fig. 1. Work function of two WO_x phases (sample A: phase made of 0.15 eqML of W; sample B: phase made of 0.25 eqML of W) (a) and low binding energy part of the valence band (photon energy = 45 eV) of sample A (b) as function of molecular oxygen exposure. Hollow signs correspond to work functions after sample preparation.

and it is hard to distinguish scans recorded after each exposure. All these results confirm the reversibility of the surface oxidation through annealing at 670 K under UHV.

To go deeper in the involved mechanisms, Ti2p, Ti3p and W4f core level spectra were also recorded on sample A after the last step of phase elaboration (i.e. an annealing at 670 K, spectrum (0)) and two subsequent cycles of exposure/annealing. Difference spectra related to the first spectrum (i.e. those recorded after phase elaboration) are also reported in the bottom part of Fig. 3 and give interesting piece of information about oxidation/reduction processes. Indeed, changes can be observed on both core level spectra indicating that both Ti and W are involved in oxidation/reduction processes. On Ti2p spectra, the main component is the Ti^{4+} contribution to Ti2p3/2 line. However, an additional component can be seen at higher binding energy (at ca. 1.7 eV from the main peak). Such a component is characteristic of Ti^{3+} ion, i.e. titanium reduced species [23]. Ti^{2+} might also be present but in quantities too low to be detectable. Anyway, this feature related to reduced titanium species clearly decreases after oxygen exposure while the Ti^{4+} component increases. After a subsequent annealing, the spectrum recovers the shape of the one before oxygen exposure, indicating that the oxidized and reduced components of Ti2p lines recover their initial values. The Ti^{3+} (and maybe Ti^{2+}) species are thus involved in the oxidation/reduction processes. Similar remark can be evoked about tungsten species. Main W4f7/2 and 5/2 lines at 33.2 eV and 35.3 eV respectively, are partially hidden by Ti3p line but are well observable. However, after oxygen exposure, the intensities of these tungsten lines slightly decrease indicating a change of tungsten chemistry such as an oxidation which is characterized by appearance of W4f components at higher binding energy as revealed by difference spectra even though these components are highly masked by the Ti3p line which occurs at a similar binding energy. Concerning the W4f7/2 and 5/2 lines, these ones are observed at 33.2 eV and 35.3 eV after annealing. These binding energies correspond to neither metallic tungsten nor W atoms bonded to adsorbed oxygen. Indeed, in such a case the W4f7/2 line should be in the 31–32 eV range [24]. Actually, W4f7/2 line binding energy rather corresponds to W^{4+} ions [25]. Moreover, according to Ref. [25], there are 1.2 eV and 2.0 eV shifts between 4+ and 5+ components and between 4+ and 6+ components, respectively. Nevertheless, even from difference spectra it is very hard to determine which component(s) appear(s) due to oxygen exposure.

It should be noticed that similar reversible oxidation process does not take place neither in case of pure titanium dioxide rutile crystal nor for tungsten oxide phases grown on silicon oxide surface. Indeed, in case of non stoichiometric TiO_2(1 1 0) surface,

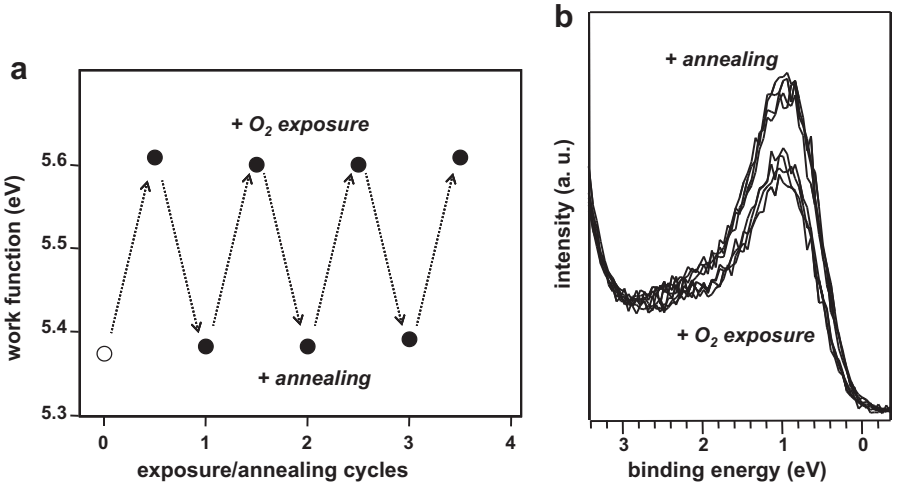

Fig. 2. Work function (a) and low binding energy part of the valence band (photon energy = 45 eV) (b) of sample A (phase made of 0.15 eqML of W) during cycles of 1 L oxygen exposure (10^{-8} Torr of O_2 for 100 s)/annealing under UHV (670 K). Hollow signs correspond to work functions after sample preparation.

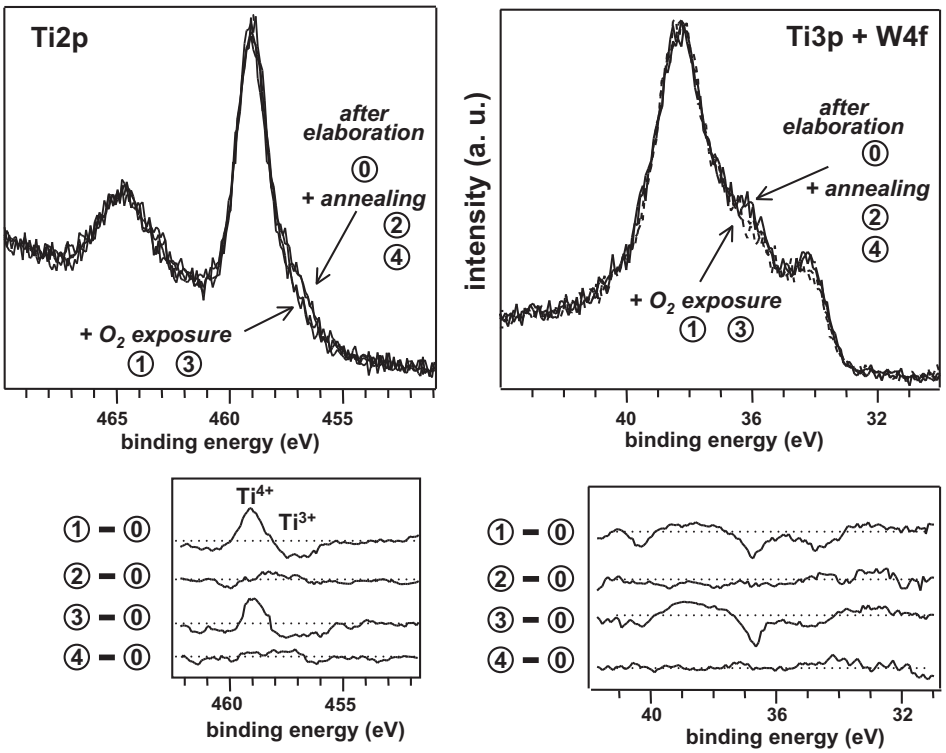

Fig. 3. Ti2p (photon energy = 510 eV) as well as Ti3p and W4f (photon energy = 150 eV) core level spectra recorded after sample elaboration (finished by an annealing at 670 K – spectrum (0)) and during cycles of O_2 exposure (1 L: 10^{-8} Torr of molecular oxygen for 100 s – spectra (1) and (3))/annealing under UHV at 670 K (spectra (2) and (4)). Difference spectra are offered in the bottom part of the figure in order to better reveal the differences induces by treatments. As the raw spectra are quite noisy, the difference spectra are obtained after smoothing of these initial scans.

oxidation cannot occur at room temperature [26] while WO_x phases elaborated on SiO_2 are progressively oxidized by cycles of oxygen exposure at RT/annealing under UHV [22]. These points support the hypothesis that reversible process is an effect of interfacial process between titanium oxide and tungsten oxide. In other words, the fact that interfacial oxygen atoms are bound to both W and Ti ions seems to drastically change the redox properties of the whole system compare to separate titanium and tungsten oxide.

3.2. Molybdenum oxide phases

As for tungsten, two MoO_x phases were studied. They were prepared according to procedure exposed in Ref. [19] using $Mo(CO)_6$ carbonyl molecules rather than $W(CO)_6$ (see Section 3.1). As for the case of tungsten, Mo amount which was deposited on substrate can be estimated from Mo3d/Ti2p area ratio, by comparison with PVD deposits [17]. These molybdenum amounts correspond to ca. 0.10 eqML for a series of samples called C and 0.35 eqML for another series of samples called D. The final treatment of all these samples consists in an annealing under UHV at 670 K. These two kinds of molybdenum oxide phases are then exposed to molecular oxygen at room temperature in successive steps through only 3 orders of magnitude from 1 to 10^3 L (2×10^3 L for sample C). Between each steps both sample work function and low binding energy part of the spectrum are recorded. These measurements are reported in Fig. 4a for the work function of the two samples and Fig. 4b for the

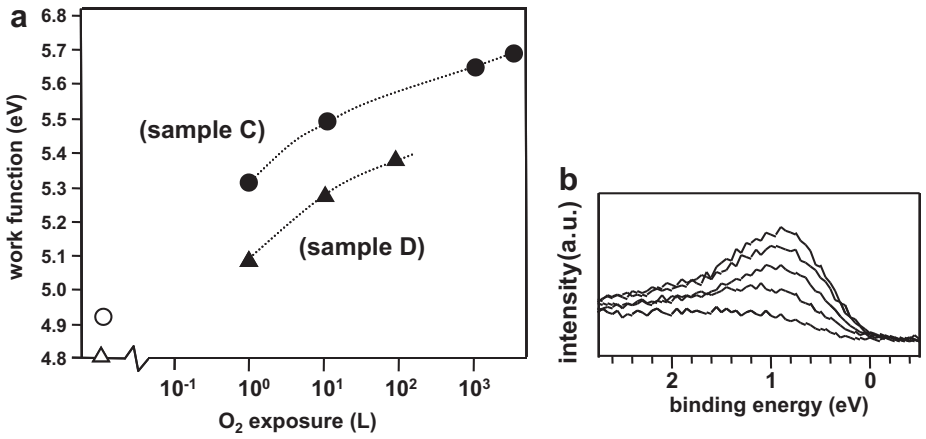

Fig. 4. Work function of two MoO_x phases (sample C: phase made of 0.1 eqML of Mo; sample D: phase made of 0.35 eqML of Mo) (a) and low binding energy part of valence band (photon energy = 45 eV) corresponding to low binding energy part of the valence band of sample C (b) as function of molecular oxygen exposure. Hollow signs correspond to work functions after sample preparation.

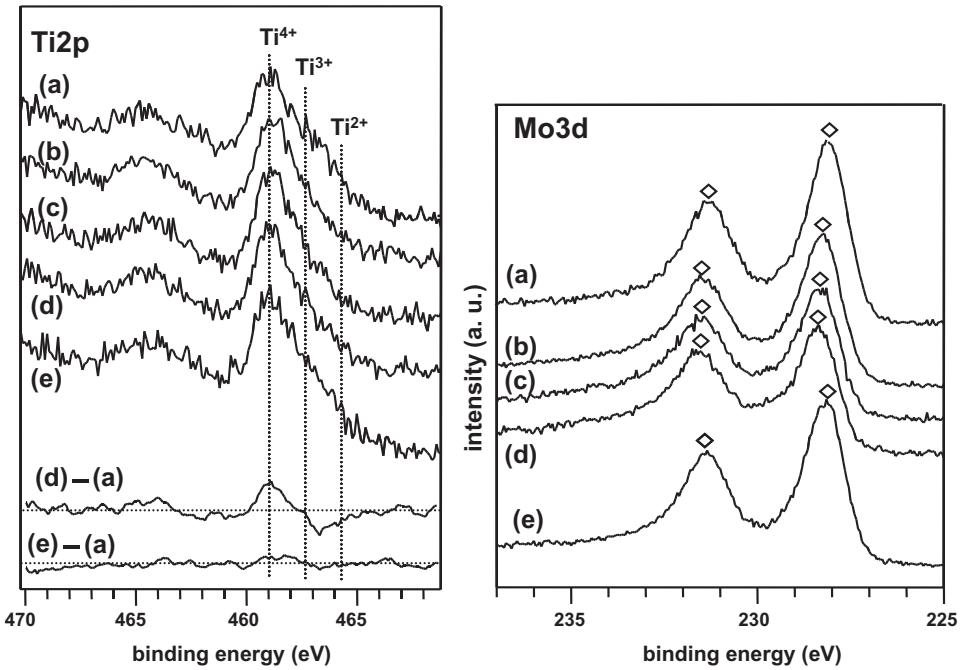

Fig. 5. Ti2p (photon energy = 510 eV) and Mo3d (photon energy = 320 eV) core level spectra recorded on sample D: after preparation of sample (a), after subsequent exposure to 1 L (b), 10 L (c) and 100 L (d) of O_2 and after annealing at 470 K (e). Difference spectra are offered for Ti2p in the bottom part of the figure in order to better reveal the differences induced by treatments. As the initial spectra are quite noisy, the difference spectra are obtained after smoothing of initial spectra.

low binding energy part of the valence band for sample C. As in the case of tungsten oxide phases, the first point corresponds to a measurement before any oxygen exposure and is not involved in curve evolution.

The evolution of work function of molybdenum oxide phases as function of oxygen exposure (Fig. 4a) has a shape very similar to the ones recorded for tungsten oxide phases even though the range of measured work function is wider in case of molybdenum oxide: for oxygen exposures going from 10^{-2} L to 10^{3} L, work function variation is 0.7 eV while it was 0.5 eV in case of tungsten oxide. In the low binding energy part of the valence band of sample C (Fig. 4b) a feature at ca. 1 eV is also observed. Such a feature, the intensity of which is function of molybdenum coverage, is composed of both Mo4d states [17] and Ti3d ones related to the interaction of molybdenum metal atoms and oxide surface. As in the case of tungsten oxides, a clear decrease in the intensity of this gap feature is observed while increasing the oxygen exposure even though for highest exposure, gap states remain less detectable than in the case of tungsten oxide. Such a feature decrease is due to sample surface oxidation. This process can be also revealed through Ti2p and Mo3d core level spectra as for instance in the case of sample D (Fig. 5). For this sample, molybdenum oxide phase elaboration leads to a noticeable reduction of titanium: Ti^{3+} and Ti^{2+} components are well evidenced in Ti2p line recorded before any oxygen exposure (Fig. 5a). During exposure (Fig. 5b–d), the features related to these components decrease as Ti^{4+} one increases. This is well shown through difference spectrum and reveals partial oxidation of titanium species. In the meanwhile, Mo3d lines shift towards higher binding energy revealing also molybdenum oxidation. Indeed, the binding energy of Mo3d5/2 line was ca. 228.0 eV before oxygen exposure, in good agreement with the standard value reported for metallic molybdenum [27] whereas this binding energy reaches 228.4 eV, i.e. a value corresponding to Mo^{2+} [27] after exposure to 100 L of molecular oxygen.

The subsequent annealing of sample at 470 K under UHV induces a further increase in intensities of Ti^{3+} and Ti^{2+} species. The Ti2p difference spectrum shows even that ratio between different titanium components are, more or less, the same than before oxygen exposure. Moreover, Mo3d lines shifts back to the positions recorded before oxygen exposure (Fig. 5e).

Besides, the surface oxidation of sample D can be completed after an exposure to air for some days as previously shown [24]. Ti2p lines exhibit then only Ti^{4+} components whereas Mo3d lines shows Mo^{6+} components and no states are observable in the band gap. Such a sample exhibits thus a semi conductor behaviour as proved by surface conduction measurements carried out under nitrogen (see in Fig. 6). Indeed, between 290 and 370 K, sample conductivity exponentially increases. However, from 370 K conduction properties begin to change. At 440 K conductivity even begins to decrease while, from 470 K this decrease becomes linear. Such a new conductivity behaviour is characteristic of metallic conduc-

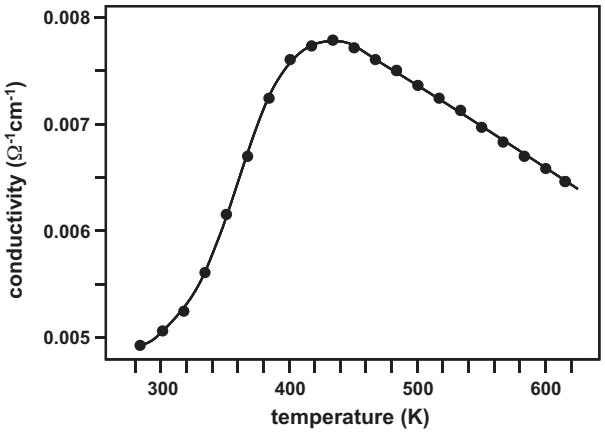

Fig. 6. Surface conductivity of sample D previously stocked under air for several days as function of temperature during an annealing under pure nitrogen. 4 probe measurements according to Van der Pauw procedure.

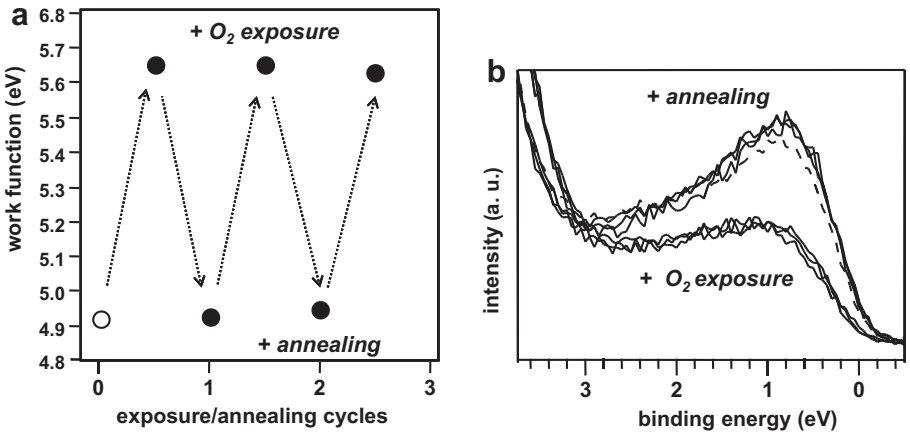

Fig. 7. Work function (a) and low binding energy part of the valence band (photon energy = 45 eV) (b) of sample C during cycles of oxygen exposure (1000 L: 100 s of O_2 at 10^{-5} Torr)/annealing under UHV (470 K). Hollow sign corresponds to work functions after sample preparation.

tivity. Besides, after cooling down to 300 K, the metallic behaviour is preserved. The conductivity mechanism changes seem clearly related to reduction of sample. Nitrogen atmosphere seems thus to act like vacuum leading to same form of sample reduction. Change in the conductivity is thus related to appearance (or disappearance) of electronic states in the band gap close to Fermi level allowing the change from a metal to a semi conductor behaviour when these states are populated or not.

From conductivity results, it appears that 470 K is an annealing temperature under nitrogen atmosphere high enough to reverse the oxidation process. By the way, an annealing at this temperature of samples C and D carried out after an oxygen exposure results in a decrease of the work functions to the initial values. The reversibility of oxidation occurs thus at lower temperature than in case of tungsten. This point, although quite puzzling, could be linked to a lessening of metal/oxygen bonds in molybdenum oxide compared to tungsten oxide.

Two cycles of exposure/annealing were also carried out on a sample C. Fig. 7 shows the evolution of work function as well as of the low binding energy part of the valence band along these cycles. As in the case of tungsten oxide phases, these experiments evidence reversibility of the oxidation phenomena. Such reversibility is also illustrated by chemical shifts recorded on Mo3d lines (Fig. 8): while oxygen exposure induces a 0.5 eV shift towards higher binding energy (for Mo3d5/2, from 228.6 eV before exposure to 229.1 eV after exposure to 1000 L), a subsequent annealing of the sample at 470 K under UHV makes the lines shifting back. For this sample, during exposure/annealing cycles, the molybdenum state seems thus oscillating between 2+/3+ state and 3+/4+ states according to different references available about different molybdenum oxidation states [27,28].

As in the case of titanium oxide/tungsten oxide system, the redox properties of titanium oxide/molybdenum oxide system are quite different to those of separate titanium and molybdenum

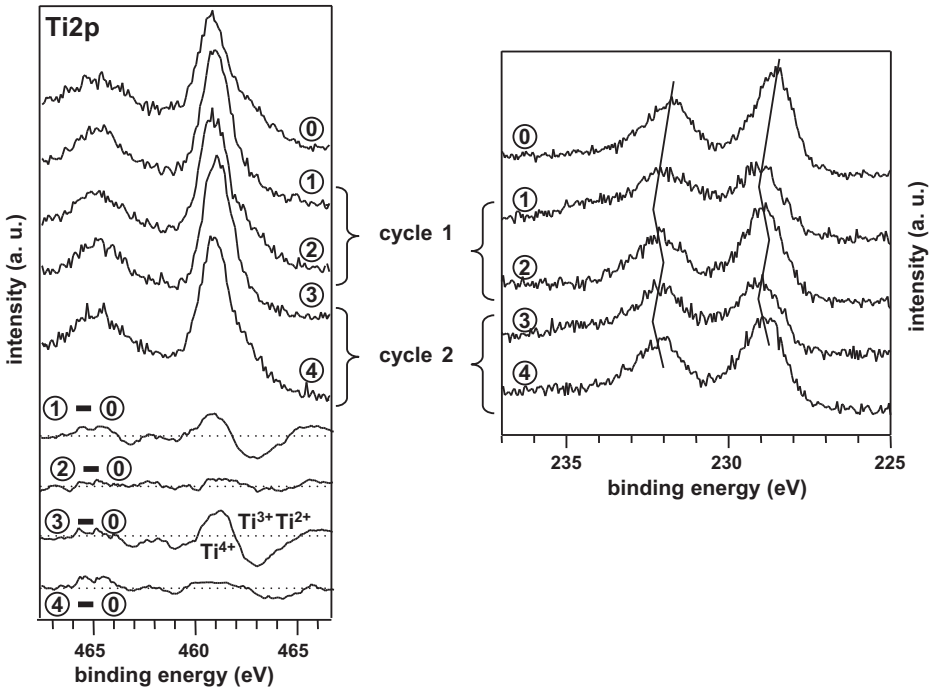

Fig. 8. Ti2p (photon energy = 510 eV) and Mo3d (photon energy = 320 eV) core level spectra recorded after sample elaboration (finished by an annealing at 670 K – spectrum (0)) and during cycles of O_2 exposure (1000 L: 100 s of O_2 at 10^{-5} Torr – spectra (1) and (3))/annealing under UHV at 670 K (spectra (2) and (4)). Difference spectra are offered in the bottom part of the figure in order to better reveal the differences induced by treatments. As the raw spectra are quite noisy, the difference spectra are obtained after smoothing of these initial scans.

oxides. Actually, the involved processes may be a kind of double adlineation process. Such a process concerns generally oxide-metal borderlines sites and allows reactions such as dissociation ones due to presence of reduced center on a support oxide around metal clusters [29]. This kind of process is observed in case of tungsten (or molybdenum) oxides (mainly WO_3 or MoO_3) when these oxides are supports of noble metal clusters [30,31] but is also revealed for titania as support [32]. In this latter case, the adlineation effect is related to Ti^{3+} centers resulting from metal/oxide interaction. In the present case, phenomenon could occur on both oxides (support and deposit) allowing dissociation of molecular oxygen inducing oxidation of the system (both substrate and deposit as well revealed) during exposure steps as well as partial decomposition of system during annealing. Besides, one should note that the involved temperatures are too low to induce diffusion of oxygen anions/oxygen vacancies into the bulk [18].

4. Conclusion

WO_x and MoO_x phases supported on TiO_2(1 1 0) surfaces constituted from fractional W or Mo coverage are partially oxidized by molecular oxygen at room temperature even for very low exposure (0.1 L). The different oxidation steps take place on a wide range of exposures (until 7 orders of magnitude). Both Ti and W (or Mo) species are involved in oxidation processes and the sample stoichiometry can be followed through work function measurement. Sample oxidation is reversible through an annealing under UHV at 670 K for tungsten oxide samples and at 470 K for molybdenum oxide. Several cycles of exposure/annealing are possible without changes in work function or stoichiometry indicating no aging of samples during these cycles.

Acknowledgements

The research leading to these results has received funding from the European Community's Seventh Framework Programme (FP7/2007-2013) under grant agreement no. 226716.

References

[1] M. Stankova, X. Vilanova, E. Llobet, L. Calderer, C. Bittencourt, J.J. Pireaux, X. Correig, Sens. Actuat. B 105 (2005) 271–277.
[2] A. Labidi, E. Gillet, R. Delamare, M. Maaref, K. Aguir, Sens. Actuat. B 120 (2006) 338–345.
[3] H. Liu, S. Huang, L. Zhang, S. Liu, W. Xin, L. Xu, Catal. Commun. 10 (2009) 544–548.
[4] D.P. Debecker, R. Delaigle, K. Bouchmella, P. Eloy, E.M. Gaigneaux, P.H. Mutin, Catal. Today 157 (2010) 125–130.
[5] B.W. Lee, H. Cho, D.W. Shin, J. Ceram. Process. Res. 8 (2007) 203–207.
[6] L. Chen, J. Li, M. Ge, R. Zhu, Catal. Today 153 (2010) 77–83.
[7] A. Mills, S. Le Hunte, J. Photochem. Photobiol. A: Chem. 108 (1997) 1–35.
[8] A.G. Agrios, P. Pichat, J. Appl. Electrochem. 35 (2005) 655–663.
[9] J.L. Gole, J.D. Stout, C. Burda, Y. Lou, X. Chen, J. Phys. Chem. B 108 (2004) 1230–1240.
[10] H. Yamashita, H. Harada, J. Misaka, M. Takeushi, K. Ikeue, M. Anpo, J. Photochem. Photobiol. A: Chem. 148 (2002) 257–261.
[11] X.Z. Li, F.B. Li, C.L. Yang, W.K. Ge, J. Photochem. Photobiol. A: Chem. 141 (2001) 209–217.
[12] X. Wang, N. Miura, N. Yamazoe, Sens. Actuat. B 66 (2000) 74–76.
[13] C. Cantalini, W. Wlodarski, Y. Li, M. Passacantando, S. Santucci, E. Comini, F. Faglia, G. Sberveglieri, Sens. Actuat. B 64 (2000) 182–188.
[14] N. Magg, J.B. Giorgi, T. Schroeder, M. Baumer, H.J. Freund, J. Phys. Chem. B 106 (2002) 8756–8761.
[15] J. Kim, O. Bondarchuk, B.D. Kay, J.M. White, Z. Dohnálek, Catal. Today 120 (2007) 186–195.
[16] S. Bourgeois, B. Domenichini, F. Sutara, V. Matolin, Vacuum 82 (2007) 146–149.
[17] B. Domenichini, G.A. Rizzi, P. Krüger, M. Della Negra, Z. Li, M. Petukhov, G. Granozzi, P.J. Møller, S. Bourgeois, Phys. Rev. B 73 (2006) 245433 (11 pp.).
[18] B. Domenichini, A.M. Flank, P. Lagarde, S. Bourgeois, Surf. Sci. 560 (2004) 63–78.
[19] J. Prunier, B. Domenichini, Z. Li, P.J. Møller, S. Bourgeois, Surf. Sci. 601 (2007) 1144–1152.
[20] K.P. Reddy, T.L. Brown, J. Am. Chem. Soc. 117 (1995) 2845–2854.
[21] B. Domenichini, J. Prunier, M. Petukhov, Z. Li, P.J. Møller, S. Bourgeois, J. Electron Spectrosc. Relat. Phenom. 163 (2008) 19–27.
[22] S. Bruyere, B. Domenichini, V. Potin, Z. Li, S. Bourgeois, Surf. Sci. 603 (2009) 3041–3048.
[23] B. Domenichini, S. Pétigny, V. Blondeau-Patissier, A. Steinbrunn, S. Bourgeois, Surf. Sci. 468 (2000) 192–202.
[24] C.H.F. Peden, N.D. Shinn, Surf. Sci. 312 (1994) 151–156.
[25] K. Masek, J. Libra, T. Skala, M. Cabala, V. Matolin, V. Chab, K.C. Prince, Surf. Sci. 600 (2006) 1624–1627.
[26] V. Blondeau-Patissier, B. Domenichini, A. Steinbrunn, S. Bourgeois, Appl. Surf. Sci. 175 (2001) 674–677.
[27] G.E. Buono-Core, G. Cabello, A.H. Klahn, A. Lucero, M.V. Nuñez, B. Torrejón, C. Castillo, Polyhedron 29 (2010) 1551–1554.
[28] Y.-Z. Wang, M. Yang, D.-C. Qi, S. Chen, W. Chen, A.T.S. Wee, X.-Y. Gao, J. Chem Phys. 134 (2011) 034706 (6 pp.).
[29] K. Hayek, R. Kramer, Z. Paál, Appl. Catal. A: Gen. 162 (1997) 1–15.
[30] C. Hoang-Van, O. Zegaoui, Appl. Catal. A: Gen. 164 (1997) 91–103.
[31] J.G. Kim, J.R. Regalbuto, J. Catal. 139 (1993) 175–190.
[32] S. Gan, Y. Liang, D.R. Baer, M.R. Sievers, G.S. Herman, C.H.F. Peden, J. Phys. Chem. B 105 (2001) 2412–2416.